Chapter 1

Topological Band Theory and the $\mathbb{Z}_2$ Invariant

C.L. Kane
Department of Physics and Astronomy, University of Pennsylvania, Philadelphia, PA 19104, USA

Chapter Outline Head

Topological Insulators. http://dx.doi.org/10.1016/B978-0-444-63314-9.00001-9

1 INTRODUCTION

A central goal in condensed matter physics is to characterize phases of matter. Some phases, such as magnets and superconductors, can be understood in terms of the symmetries that they spontaneously break. In recent decades, it has become apparent that there can exist a more subtle kind of order in the pattern of entanglement in a quantum ground state. The concept of topological order was introduced to describe the quantum Hall effect [1,2]. The quantum Hall state does not break any symmetries, but it has fundamental properties (such as the quantized Hall conductivity, and the number of conducting edge modes) that are insensitive to smooth changes in materials parameters and cannot change unless the system passes through a quantum phase transition. These properties can be understood as consequences of the topological structure of the quantum state.

While the topological characterization of the quantum Hall effect is an old story, interest in topological order has been rekindled by the discovery of topological insulators [3–13]. A topological insulator, like an ordinary insulator, has a bulk energy gap separating the highest occupied electronic band from the lowest empty band. The surface (or edge in two dimensions) of a topological insulator, however, necessarily has gapless electronic states that are protected by time reversal symmetry. Like the integer quantum Hall state, which has unique gapless chiral edge states [14], the surface (or edge) states of a topological insulator are topologically protected and exhibit a conducting state with properties that are unlike any other known 1D or 2D electronic systems.

The concept of topological order [2] is often used to characterize fractional quantum Hall states [15], which require an inherently many body approach to understand [16]. However, topological considerations also apply to the simpler integer quantum Hall states [1], for which an adequate description can be formulated in terms of single particle quantum mechanics. In this regard, topological insulators are similar to the integer quantum Hall effect. Due to the presence of a single particle energy gap, electron-electron interactions do not modify the state in an essential way. The phenomenology of topological insulators can be understood in the framework of the band theory of solids [17]. It is remarkable that after more than 80 years, there are still treasures to be uncovered within band theory.

In this chapter we will provide a pedagogical introduction to the foundations of topological band theory and explain how these ideas can be used to characterize the integer quantum Hall effect and topological insulators.

2 TOPOLOGY AND BAND THEORY

We begin by reviewing the key elements of topology and band theory. We will introduce the notion of topological equivalence and explain its role in band theory, and we will describe the deep connection between the bulk topology

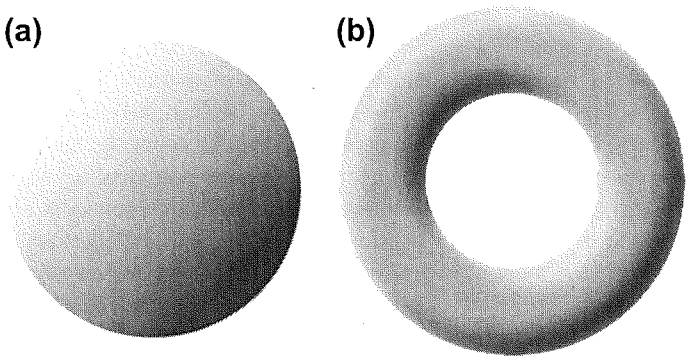

FIGURE 1 The surfaces of a sphere ($g = 0$) and a doughnut ($g = 1$) are distinguished topologically by their genus g.

and protected boundary modes. In Section 2.3. We will discuss the Berry phase, which is a key conceptual tool for the analysis of topological phenomena.

2.1 Topology

Topology is a branch of mathematics concerned with geometrical properties objects that are insensitive to smooth deformations. This is most easily illustrated by the simple example of closed two-dimensional surfaces in three dimensions (see Fig. 1). A sphere can be smoothly deformed into many different shapes, such as the surface of a disk or a bowl. But a sphere cannot be smoothly deformed into the surface of a doughnut. A sphere and a doughnut are distinguished by an integer topological invariant called the genus, g, which is essentially the number of holes. Since an integer cannot change smoothly, surfaces with different genus cannot be deformed into one another, and are said to be topologically distinct. Surfaces that can be deformed into one another are topologically equivalent. Determining the topological invariants that characterize a given object is an interesting math problem. For surfaces, a beautiful theorem, known as the Gauss-Bonnet theorem, states that the integral of the Gaussian curvature, K over a surface defines an integer topological invariant called the Euler characteristic [18],

$$\chi = \frac{1}{2\pi}\int_S K dA. \tag{1}$$

It can easily be checked that $\chi = 2$ for a sphere of radius R, where $K = 1/R^2$. More generally, the Euler characteristic is quantized and related to the genus by $\chi = 2 - 2g$. The topological invariants that we will be concerned with in this chapter are similar, though they will characterize more abstract objects.

2.2 Band Theory

How can topology be used to characterize phases of matter? Here we will explain the topological classification of insulators. An insulator is a material that has an energy gap for electronic excitations, which separates the ground state from all excited states. This allows for a notion of topological equivalence based on the principle of adiabatic continuity. Insulators are equivalent if they can be changed into one another by slowly changing the Hamiltonian, such that the system always remains in the ground state. Such a process is possible if there is an energy gap E_G, which sets a scale for how slow the adiabatic process must be. Thus, insulators are topologically equivalent if there exists an adiabatic path connecting them along which the energy gap remains finite. It follows that connecting topologically inequivalent insulators necessarily involves a phase transition, in which the energy gap vanishes.

The topological classification of general gapped many body states is a formidable problem that has not been completely solved. A tremendous simplification occurs if we consider a subclass of states that can be described by the band theory of solids. Such band insulators can be effectively described in the independent electron approximation, where the many body ground state is represented as a Slater determinant of single particle states. This does not mean that electron interactions are being ignored. The existence of an energy gap means that the many body state remains topologically equivalent when finite strength interactions are turned on. We thus assume that the state in question can be adiabatically connected to noninteracting electrons, and topologically classify the band structures. It is then important to address whether the topological distinctions found within band theory persist when interactions are added. We shall see that this is indeed the case.

A second key assumption we will make in this chapter is that the material is crystalline, which allows us to take advantage of translation symmetry. This assumption can be relaxed, and we will touch on the issue of disorder later in this chapter. Translation symmetry allows the single particle states to be labeled by their crystal momentum $\mathbf{k}$. According to Bloch's theorem, they may be written $|\psi(\mathbf{k})\rangle = e^{i\mathbf{k}\cdot\mathbf{r}}|u(\mathbf{k})\rangle$, where $|u(\mathbf{k})\rangle$ is a cell periodic eigenstate of the Bloch Hamiltonian,

$$H(\mathbf{k}) = e^{i\mathbf{k}\cdot\mathbf{r}} H e^{-i\mathbf{k}\cdot\mathbf{r}}. \tag{2}$$

$H(\mathbf{k})$, or equivalently its eigenvalues $E_n(\mathbf{k})$ and eigenvectors $|u_n(\mathbf{k})\rangle$, defines the band structure. An insulating band structure has an energy gap separating the highest occupied band from the lowest empty band. Lattice translation symmetry implies $H(\mathbf{k}+\mathbf{G}) = H(\mathbf{k})$ for reciprocal lattice vectors $\mathbf{G}$. The crystal momentum is therefore defined in the periodic Brillouin zone, with $\mathbf{k} \equiv \mathbf{k}+\mathbf{G}$, which has the topology of a torus T^d in d dimensions. Thus, an insulating band structure can be viewed as a mapping from the Brillouin zone torus to the space of Bloch Hamiltonians with an energy gap.

2.3 Topological Band Theory and the Bulk-Boundary Correspondence

One of the objects of topological band theory is to classify topologically distinct Hamiltonians $H(\mathbf{k})$. By doing so, we are classifying distinct electronic phases. The most important consequence of this occurs when there is a spatial interface between two topologically distinct phases. Imagine an interface where a crystal slowly interpolates as a function of distance y between a two topologically distinct phases. Somewhere along the way the energy gap has to go to zero, because otherwise the two phases would be equivalent. There will therefore be low energy electronic states bound to the region where the energy gap passes through zero.

A second object of topological band theory is thus to characterize those gapless states. We will see that they too can be classified topologically, and that there is a deep principle, which we will refer to as the bulk-boundary correspondence, which relates the boundary topological invariants to the difference in the bulk topological invariants. This interplay between topology and gapless modes is a ubiquitous phenomenon in physics, and has appeared in many contexts [19,21–24].

2.4 Berry Phase, and the Chern Invariant

A key role in topological band theory is played by the Berry phase [25]. The Berry phase arises because of the intrinsic phase ambiguity of a quantum mechanical wavefunction. The Bloch states are invariant under the transformation

$$|u(\mathbf{k})\rangle \rightarrow e^{i\phi(\mathbf{k})}|u(\mathbf{k})\rangle. \tag{3}$$

This transformation is reminiscent of an electromagnetic gauge transformation, and invites the definition of the Berry connection,

$$\mathbf{A} = -i\langle u(\mathbf{k})|\nabla_{\mathbf{k}}|u(\mathbf{k})\rangle. \tag{4}$$

$\mathbf{A}$ is similar to the electromagnetic vector potential. Under (3) it transforms as $\mathbf{A} \rightarrow \mathbf{A} + \nabla_{\mathbf{k}}\phi(\mathbf{k})$. Though $\mathbf{A}$ is not gauge invariant, the analog of magnetic flux is. For any closed loop C in $\mathbf{k}$ space, we may define the Berry phase,

$$\gamma_C = \oint_C \mathbf{A}\cdot d\mathbf{k} = \int_S \mathcal{F} d^2\mathbf{k}, \tag{5}$$

where $\mathcal{F} = \nabla \times \mathbf{A}$ defines the Berry curvature. For notational simplicity, we will assume here that $\mathbf{k}$ is two dimensional. The generalization to higher dimensions is straightforward.

The Berry phase has many applications in physics, and describes the phase acquired under an adiabatic cycle. In the present context, it will be useful for classifying loops in momentum space. In the following section we will attach physical meaning to it.

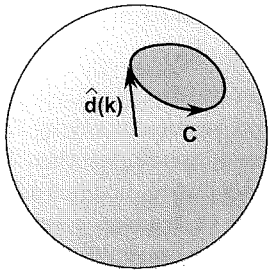

FIGURE 2 The Berry phase in a two band theory is given by half the solid angle swept out by $\hat{\mathbf{d}}(\mathbf{k})$.

It is useful to understand the Berry phase for the simplest two level Hamiltonian, which may be expressed in terms of Pauli matrices $\vec{\sigma}$ as

$$H(\mathbf{k}) = \mathbf{d}(\mathbf{k}) \cdot \vec{\sigma} = \begin{pmatrix} d_z & d_x - id_y \\ d_x + id_y & -d_z \end{pmatrix}. \tag{6}$$

This Hamiltonian has eigenvalues $\pm|\mathbf{d}|$. We ignore a term proportional to the identity because that does not affect the eigenvectors, which depend only on the unit vector $\hat{\mathbf{d}} = \mathbf{d}/|\mathbf{d}|$. $\hat{\mathbf{d}}$ can be viewed as a point on a sphere S^2.

A classic result, shown by Berry [25], is that for a loop C the phase associated with the ground state, obtained from (4) and (5) is (see Fig. 2)

$$\gamma_C = \frac{1}{2}\left(\text{Solid angle swept out by } \hat{\mathbf{d}}(\mathbf{k})\right). \tag{7}$$

In particular, when C corresponds to a 2π rotation of $\hat{\mathbf{d}}$ in a plane, the Berry phase is π. The Berry curvature is given by the solid angle per unit area in $\mathbf{k}$ space, which is simply half the solid angle element for the mapping $\hat{\mathbf{d}}(\mathbf{k})$,

$$\mathcal{F} = \frac{1}{2}\epsilon_{ij}\hat{\mathbf{d}} \cdot (\partial_i \hat{\mathbf{d}} \times \partial_j \hat{\mathbf{d}}). \tag{8}$$

An important consequence of (8) is that the Berry curvature integrated over a closed 2D space (such as a 2D Brillouin zone T^2) is a multiple of 2π that is equal to the number of times $\hat{\mathbf{d}}(\mathbf{k})$ wraps around the sphere as a function of $\mathbf{k}$. This defines a topological invariant called the Chern number [18], which for a closed surface S may be expressed as

$$n = \frac{1}{2\pi}\int_S \mathcal{F} d^2\mathbf{k}. \tag{9}$$

The quantization of the Chern number is more general than the two band model, and follows from the fact that for a loop C on a closed surface, the "inside" of C used in (5) is arbitrary, so that the surface integral over the inside and the outside

must agree with one another up to a multiple of 2π. It follows that the Berry curvature integrated over the entire surface must be $2\pi n$. This quantization is also closely related to the quantization of the Dirac magnetic monopole. Note the similarity with (1). $\mathcal{F}$ can be viewed as a curvature, similar to the Gaussian curvature K.

In the following sections we will discuss the physical meaning and consequences of this and other topological invariants.

3 ILLUSTRATIVE EXAMPLE: POLARIZATION AND TOPOLOGY IN ONE DIMENSION

In this section we will consider the simplest setting for topological band theory, which is one dimension. This will allow us to introduce several key concepts in their simplest form, including the electric polarization, the Chern number, and topologically protected boundary states. We will introduce the Su, Schrieffer Heeger (SSH) [20] model, which provides a simple and solvable theory that illustrates these ideas.

3.1 Polarization as a Berry Phase

In elementary electrostatics, the electric polarization $\mathbf{P}$ is defined as the dipole moment per unit volume. Polarization leads to bound charges in the bulk $\rho_b = -\nabla \cdot \mathbf{P}$ and on the surface $\sigma_b = \mathbf{P} \cdot \hat{n}$. In one dimension, the polarization P is related to the end charge,

$$Q_{\text{end}} = P. \tag{10}$$

In this section, we show how to determine the polarization from a 1D band structure. The problem is not trivial because a band structure is generally defined on a system with periodic boundary conditions, so Q_{end} is inaccessible. The solution, which has emerged in the theory of ferroelectricity [26–29], provides a beautiful application of Berry's phase. The 1D polarization is the Berry phase of the occupied Bloch wavefunctions around the 1D Brillouin zone,

$$P = \frac{e}{2\pi} \oint_{BZ} A(k) dk. \tag{11}$$

The integral is over the 1D Brillouin zone, which is equivalent to a circle S^1. Detailed derivations of (11) can be found in the literature. Here we will motivate the result using physical arguments.

The first piece of circumstantial evidence is that both the polarization and the Berry phase share a similar intrinsic ambiguity. Q_{end} in (10) is not completely determined because integer charges can be added or removed from the ends without changing the bulk. Thus, $Q_{\text{end}} = P \mod e$. P in (11) has a similar

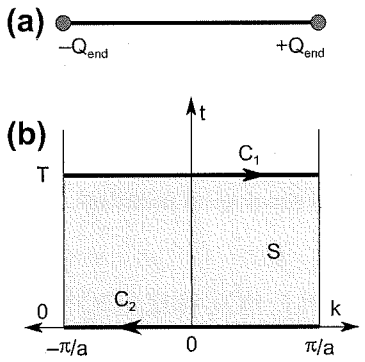

FIGURE 3 (a) The polarization in 1D determines the end charge modulo e. (b) The change in the polarization is given by the difference of Berry phases on loops C_1 and C_2.

ambiguity because under a gauge transformation $|u(k)\rangle \to e^{i\phi(k)}|u(k)\rangle$ with $\phi(\pi/a) - \phi(-\pi/a) = 2\pi n, P \to P + ne$. At first sight, this appears to violate (5), which implies γ_C is gauge invariant. However, it must be noted that the 1D Brillouin zone defines a special kind of loop that is not the boundary of an interior, so that the reasoning in (5) does not apply. On such nontrivial loops, γ_C changes by $2\pi n$ under "large" gauge transformations, in which the phase winds by $2\pi n$ around the hole.

Though the polarization and the Berry phase are both ambiguous up to an integer, *changes* in either quantity are well defined and gauge invariant. Imagine that the band structure is a function of a control parameter t. Then the change in the polarization between $t = 0$ and $t = T$ is

$$\begin{aligned}\Delta P = P_{t=T} - P_{t=0} &= \frac{e}{2\pi}\left[\oint_{C_1} - \oint_{C_2}\right]\mathbf{A}\cdot dk \\ &= \frac{e}{2\pi}\int_S \mathcal{F}\, dk\, dt. \end{aligned} \tag{12}$$

In this case, as shown in Fig. 3, $C_1 - C_2$ is the boundary of an interior, so Stokes' theorem can be used to express the integral in terms of the gauge invariant Berry curvature $\mathcal{F}$.

A second piece of circumstantial evidence is that the polarization is something like the expectation value of er, while the Berry phase is something like the expectation value of $2\pi i\nabla_k$, so if you are willing to believe $r \sim i\nabla_k$ the equality follows. This is not convincing, though, because neither $\langle r\rangle$ nor $\langle i\nabla_k\rangle$ are defined for extended Bloch states. A somewhat more rigorous version of this argument is to introduce a basis of localized Wannier states associated with lattice sites R [28],

$$|\phi(R)\rangle = \oint_{BZ}\frac{dk}{2\pi}e^{-ik(R-r)}|u(k)\rangle. \tag{13}$$

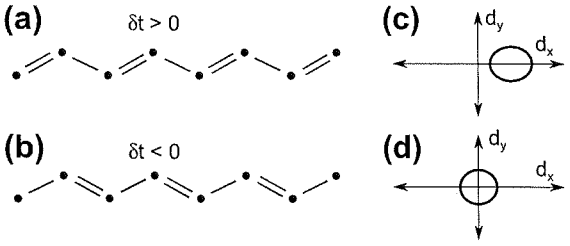

FIGURE 4 (a,b) The two distinct groundstates of the SSH model. Figures (c) and (d) show the unit vector $\hat{\mathbf{d}}(k)$.

The Wannier states depend on the gauge choice for $|u(k)\rangle$, but for a sufficiently smooth gauge they are localized so that $\langle r\rangle$ is well defined. The polarization can then be written

$$P = e\langle\phi(R)|r - R|\phi(R)\rangle = \frac{ie}{2\pi}\oint dk\langle u(k)|\nabla_k|u(k)\rangle. \tag{14}$$

3.2 Su, Schrieffer, Heeger Model

In this section we consider an important model that illustrates the analysis of the preceding sections. It will also provide a setting for introducing domain wall states. The Su Schrieffer Heeger (SSH) [20] model was introduced as a model of the conducting polymer polyacetylene, which at half filling undergoes a Peierls instability to a dimerized state. What makes this interesting is that, as shown in Fig. 4, there are two different dimerized states. We will see that there is a sense in which these two states are topologically distinct (and a sense in which they are not). Importantly, interfaces between the two states are associated with zero energy boundary states. The SSH model provides the simplest two band model for describing these topological phenomena.

To model polyacetylene, SSH introduced a 1D tight binding model

$$H = \sum_i (t + \delta t)c^\dagger_{Ai}c_{Bi} + (t - \delta t)c^\dagger_{Ai+1}c_{Bi} + h.c. \tag{15}$$

Here we have arbitrarily defined a unit cell with two atoms, labeled A and B. The dimerization is characterized by δt, which leads to an energy gap. The two dimerization patterns are distinguished by the sign of δt. For simplicity, we consider spinless electrons here (even though the real SSH model includes spin). The filling is one electron per unit cell.

To analyze (15) we Fourier transform and write

$$H = \sum_k H_{ab}(k)c^\dagger_{ak}c_{bk}, \tag{16}$$

where

$$H(k) = \mathbf{d}(k)\cdot\vec{\sigma} \tag{17}$$

and

$$\begin{aligned} d_x(k) &= (t+\delta t) + (t-\delta t)\cos ka, \\ d_y(k) &= (t-\delta t)\sin ka, \\ d_z(k) &= 0. \end{aligned} \tag{18}$$

Viewing the two band $H(k)$ in terms of $\mathbf{d}$, it is important to note that $d_z = 0$. It follows that $H(k)$ possesses a "chiral" symmetry defined by the operator $\Pi = \sigma^z$, which *anticommutes* with the Hamiltonian: $\{H(k), \Pi\} = 0$. This chiral symmetry leads to a particle-hole symmetric spectrum because any eigenstate $|u_E\rangle$ with energy E has a partner $|u_{-E}\rangle = \Pi|u_E\rangle$ with energy $-E$. This symmetry is not intrinsic, though, and will be violated in real polyacetylene (for example by second neighbor hopping). Nonetheless, it is useful to consider its effects.

Consider the polarization, which can be expressed in terms of the Berry phase using (4) and (11). For $\delta t > 0$, $d_x(k) > 0$ for all k so $\hat{\mathbf{d}}(k)$ sweeps out no solid angle, and $P = 0$. For $\delta t < 0$, however, $d_x(k \sim \pi/a) < 0$, so that $\hat{\mathbf{d}}(k)$ rotates by 2π leading to Berry phase π and $P = e/2$. The polarization can be understood easily in the strong coupling limit, $|\delta t| = t$, in which electrons reside in localized states on the strong bonds. It is clear that passing from the $\delta t = +t$ state to the $\delta t = -t$ state involves moving each electron over by half a unit cell, resulting in a polarization $e/2$.

In the presence of the chiral symmetry, the polarization must be a multiple of $e/2$. On the other hand, if the symmetry constraint is relaxed, then $\mathbf{d}$ can tip out of the xy plane, and the polarization can vary continuously. Thus, in general, there is no topology in 1D: all 1D insulating band structures are topologically equivalent. But imposing chiral symmetry leads to topologically distinct states that are distinguished by their quantized polarization. To get from the $\delta t > 0$ state to the $\delta t < 0$ state without violating the chiral symmetry requires a point where $\mathbf{d}$ vanishes, signifying a quantum phase transition. This is an example of the general principle that enhanced symmetry can lead to richer topological structure.

Real polyacetylene does not have chiral symmetry, but it does have the spatial symmetry of inversion about the center of a bond. This is expressed by $H(-k) = \sigma^x H(k)\sigma^x$, and leads to a quantized polarization, even in the absence of chiral symmetry. The SSH model also resembles the Bogoliubov-de Gennes Hamiltonian for a one-dimensional topological superconductor. In that case there is an intrinsic particle-hole symmetry, expressed by $H(-k) = -\sigma^z H(k)^* \sigma^z$, which also leads to distinct topological phases.

3.3 Domain Wall States and the Jackiw Rebbi Model

The interface between the two ground states of polyacetylene gives rise to a soliton state with a polarization charge $\pm e/2$ on the boundary. The electronic structure in the presence of such a domain wall has a zero energy midgap state.

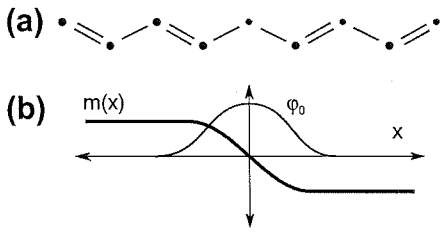

FIGURE 5 (a) A domain wall in the SSH model. (b) The midgap state is associated with a change in sign of the mass m.

The $\pm e/2$ states arise when this "zero mode" is empty/occupied. The existence of the zero mode is easily understood in the strong coupling limit $|\delta t| = t$, since there is an unpaired site on the boundary, as shown in Fig. 5(a). This state is protected in the sense that it is impossible to get rid of it without closing the bulk energy gap. Its existence can be traced to the fact that it is on an interface between topologically distinct states. Such topological zero modes were first found in a 1D field theory by Jackiw and Rebbi [19], who presented a simple exact solution for the zero mode. The SSH model provides a physical realization of the Jackiw Rebbi model.

Here we will present the Jackiw Rebbi solution, starting from the SSH model (15). The chiral symmetry $\{\Pi, H(k)\} = 0$ implies that eigenstates come in pairs at $\pm E$. It is possible, however, for a state at $E = 0$ to be its own partner, $|u_0\rangle = \Pi|u_0\rangle$. If this is the case, then this zero mode is topologically protected, because to move it away from $E = 0$ would require another state to appear out of nowhere.

To explicitly construct this zero mode, it is helpful to develop a low energy continuum theory for (15). We consider the limit $\delta t \ll t$ and focus on the low energy states near $k = \pi/a$. We thus let $k = \pi/a + q$ and expand for small q. In real space we then let $q \to -i\partial_x$. This results in a low energy Hamiltonian of the form

$$H = -iv_F\sigma^x\partial_x + m\sigma^y, \tag{19}$$

where $v_F = ta$ and $m = 2\delta t$. This Hamiltonian has the form of a massive 1 + 1D Dirac Hamiltonian, with spectrum $E(q) = \pm\sqrt{(v_F q)^2 + m^2}$.

To describe the zero mode we allow m to vary spatially with a kink such that $m(x \to +\infty) < 0$ and $m(x \to -\infty) > 0$, as shown in Fig. 5(b). A zero energy solution $H|u\rangle = 0$ can easily be constructed by multiplying on the left by $i\sigma^x$ and considering eigenstates $|z\pm\rangle$ of σ^z with eigenvalue ± 1. Integrating the resulting first-order equation leads to a single normalizable solution,

$$\psi_0(x) = e^{-\int_0^x m(x')/v_F}|z+\rangle. \tag{20}$$

This zero mode is topological in that it does not depend on the precise form of $m(x')$. It only depends on the sign change. It is guaranteed to be at zero energy if

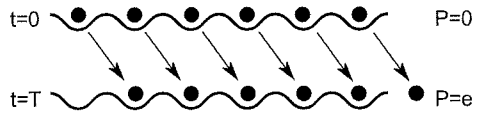

FIGURE 6 In a Thouless charge pump the polarization changes by e in each cycle.

there is chiral or particle-hole symmetry. The antikink with $\pm m(x \to \pm\infty) > 0$ is similar, but involves $|z-\rangle$.

3.4 Thouless Charge Pump, and the Chern Invariant

We have seen that without extra symmetries, such as chiral symmetry, particle-hole symmetry, or inversion symmetry there are no topological band structures in one dimension. In this section we describe another topological phenomenon that occurs in 1D in the absence of symmetries.

Consider a one-dimensional insulating Hamiltonian that changes with time adiabatically in a cyclic manner, so that $H(k,t) = H(k,t+T)$. At every time t, the system has a polarization P, that is well defined up to an integer charge e. As t changes, the change in P is completely defined. After one full cycle, the Hamiltonian returns to its original value. However, since the polarization is only defined modulo e it is possible that the polarization changes by

$$\Delta P = ne \tag{21}$$

for integer n (see Fig. 6). Such a system defines a topological charge pump [30,31], in which n electrons are transported across the system in every cycle, despite the fact that the energy gap remains finite.

In Section 3.1, we showed that the change in the P in one cycle, given by 12, is related to the Berry curvature integrated for $-\pi/a < k < \pi/a$ and $0 < t < T$. Since $H(t) = H(t+T)$, t is defined on a circle. Thus, the domain of integration of the surface integral in (12) is the 2-torus, T^2 defined by k and t. It follows that the integer n in (21) is the Chern number, defined in (9),

$$n = \frac{1}{2\pi}\int_{T^2} \mathbf{F}\, dk\, dt. \tag{22}$$

We thus conclude that the cyclic families of 1D insulators defined by $H(k,t)$ are classified by the Chern number, and that topological invariant characterizes the quantized charge pumped per cycle.

4 INTEGER QUANTUM HALL EFFECT

The integer quantum Hall effect occurs when a two-dimensional electron gas is placed in a strong perpendicular magnetic field [32]. The quantization of the

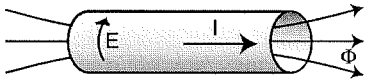

FIGURE 7 Laughlin's argument shows that when flux $\phi_0 = h/e$ is threaded down the cylinder the polarization changes by e.

electrons' circular orbits leads to quantized Landau levels. If n Landau levels are filled and the rest are empty, then an energy gap separates the occupied and empty states just as in an insulator. Unlike an insulator, though, an electric field causes the cyclotron orbits to drift, leading to a Hall current characterized by the quantized Hall conductivity, $\sigma_{xy} = ne^2/h$.

Landau levels can be viewed as a band structure. Since the generators of translations do not commute with one another in a magnetic field, electronic states cannot be labeled with momentum. However, if a unit cell with area hc/eB enclosing a flux quantum is defined, then lattice translations do commute, so Bloch's theorem allows states to be labeled by the 2D crystal momentum $\mathbf{k}$. In the absence of a periodic potential, the energy levels are simply the $\mathbf{k}$ independent Landau levels. In the presence of a periodic potential with the same lattice periodicity, the energy levels will disperse with $\mathbf{k}$. This leads to a band structure that looks identical to that of an ordinary insulator. What is the difference between the quantum Hall state and the ordinary insulator? They are distinguished by topology.

4.1 Laughlin Argument, and the TKNN Invariant

In an important 1982 paper, Thouless, Kohmoto, Nightingale, and den Nijs (TKNN) [1] showed that the integer in the integer quantized Hall conductivity is precisely the Chern number. Their calculation was a straightforward application of linear response theory, which showed that the Kubo formula for σ_{xy} is identical to (9). Rather than repeat their analysis here, we will give a slightly different physical motivation for this result, which relates it to the quantized charge pump discussed in Section 3.4.

The key insight is provided by Laughlin's argument for the integer quantum Hall effect [33]. Suppose we have an integer quantum Hall state on a cylinder and we adiabatically turn up the magnetic flux Φ threading the cylinder from 0 to the flux quantum $\phi_0 = h/e$ (see Fig. 7). The changing flux induces a Faraday electric field $d\Phi/dt$ going around the cylinder, which in turn generates a Hall current $I = \sigma_{xy} d\Phi/dt$ going down the cylinder. At the end, a net charge $\sigma_{xy} h/e$ has been transported from one end to the other. When $\Phi = \phi_0$, the vector potential can be eliminated by a gauge transformation, so that the Hamiltonian has returned to its original form at $\Phi = 0$. It follows that the charge transferred must be an integer number of electrons $Q = ne$, from which the quantization $\sigma_{xy} = ne^2/h$ follows.

Viewed as a 1D system, the cylinder with threaded magnetic flux is precisely a Thouless charge pump with $t = \Phi$. The Chern number characterizing the pump

can be evaluated by summing over all of the occupied one-dimensional subbands of the cylinder with radius R. These are indexed by a discrete azimuthal momentum $k_y^m(\Phi) = (m + \Phi/\phi_0)/R$. From (22), we find

$$n = \sum_m \frac{1}{2\pi} \int_0^{\phi_0} d\Phi \int dk_x \mathbf{F}(k_x, k_y^m(\Phi)). \tag{23}$$

Changing variables from Φ to k_y^m, it can be checked that the sum of integrals becomes a single integral over the 2D Brillouin zone $S = T^2$, given by (9).

4.2 Haldane Model

An example of the quantum Hall effect in a band theory is provided by a simple model of graphene in a periodic magnetic field introduced by Haldane [34]. This model is important because it provides a simple 2 band description of the quantum Hall effect. It also provides a stepping stone to the 2D quantum spin Hall insulator.

Graphene is a 2D form of carbon that is a material of high current interest due to experimental advances [35–38]. What makes graphene interesting electronically is the fact that the conduction band and valence band touch each other at two distinct points in the Brillouin zone. Near those points the electronic dispersion is linear, and resembles the dispersion of massless relativistic particles, which are described by the Dirac equation [39,40].

The simplest theory of graphene is a tight binding model that takes into account the p_z orbitals of each atom on a 2D honeycomb lattice.

$$H_0 = -t \sum_{<ij>} c_i^\dagger c_j. \tag{24}$$

Since there are two atoms per unit cell, this leads to a two band model (ignoring spin) that can be expressed in the form of (16, 17) with

$$\begin{aligned} d_x(\mathbf{k}) &= -t \sum_{p=1}^{3} \cos \mathbf{k} \cdot \mathbf{a}_p, \\ d_y(\mathbf{k}) &= -t \sum_{p=1}^{3} \sin \mathbf{k} \cdot \mathbf{a}_p, \\ d_z(\mathbf{k}) &= 0. \end{aligned} \tag{25}$$

Here $\mathbf{a}_1 = a(0,1)$ and $\mathbf{a}_{2,3} = a(\pm\sqrt{3}/2, -1/2)$ are the three nearest neighbor vectors pointing from the A sublattice to the B sublattice. The combination of inversion ($\mathcal{P}$) and time reversal ($\mathcal{T}$) symmetry requires $d_z(\mathbf{k}) = 0$. $\mathcal{P}$ takes $d_z(\mathbf{k})$ to $-d_z(-\mathbf{k})$, while $\mathcal{T}$ takes $d_z(\mathbf{k})$ to $+d_z(-\mathbf{k})$. An important consequence of this is that there can exist point zeros of $\mathbf{d}(\mathbf{k})$. These occur at the two distinct

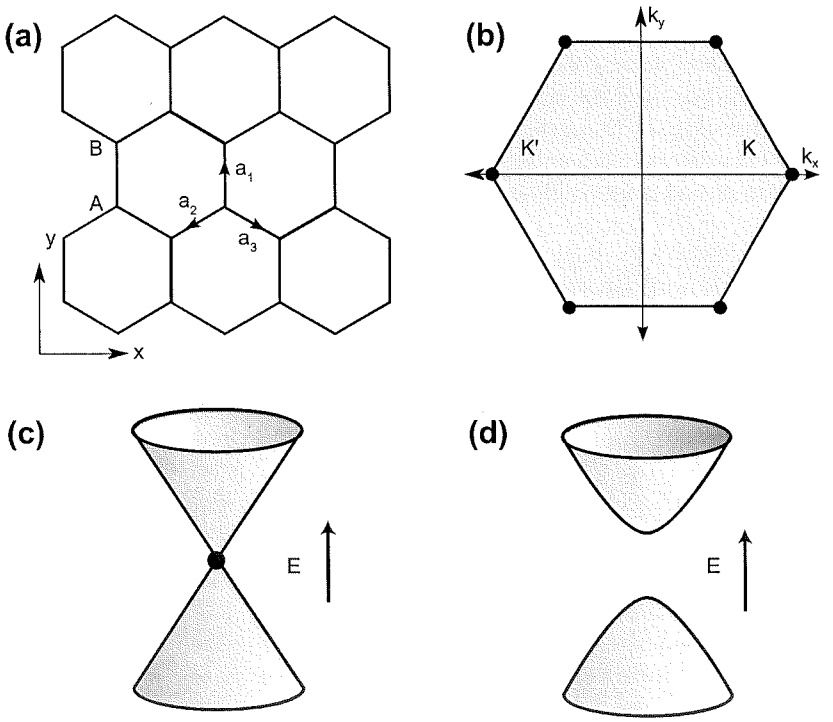

FIGURE 8 (a) Graphene's honeycomb lattice. (b) Graphene's Brillouin zone with two distinct corners **K** and **K**′. (c) Massless Dirac spectrum. (d) Massive Dirac spectrum.

corners $\mathbf{K} = (4\pi/3\sqrt{3}a, 0)$ and $\mathbf{K}' = -\mathbf{K}$ of the hexagonal Brillouin zone. For small $\mathbf{q} \equiv \mathbf{k} - \mathbf{K}$, $\mathbf{d}(\mathbf{q}) = v_F \mathbf{q} \cdot \vec{\sigma}$, with $\hbar v_F = 3ta/2$. Taking $\mathbf{q} \to -i\nabla$, the continuum theory has the form of a 2D massless Dirac Hamiltonian,

$$\mathcal{H} = -i\hbar v_F(\sigma^x \tau^z \partial_x + \sigma^y \partial_y), \tag{26}$$

which has a linear dispersion $E(\mathbf{q}) = \pm\hbar v_F|\mathbf{q}|$ shown in Fig. 8(c). Here we have introduced $\tau^z = \pm 1$ to represent states near $\mathbf{K}/\mathbf{K}'$. The degeneracy at $\mathbf{q} = 0$ is protected by $\mathcal{P}$ and $\mathcal{T}$ symmetry. By breaking these symmetries the degeneracy can be lifted. For instance, $\mathcal{P}$ symmetry is violated if the two atoms in the unit cell are inequivalent. This leads to a nonzero $\mathbf{k}$ independent

$$d_z^{\mathrm{CDW}}(\mathbf{k}) = \lambda_{\mathrm{CDW}}. \tag{27}$$

If λ_{CDW} is small, then the continuum theory acquires a mass term,

$$\Delta\mathcal{H}^{\mathrm{CDW}} = m_{\mathrm{CDW}}\sigma^z, \tag{28}$$

with $m_{\mathrm{CDW}} = \lambda_{\mathrm{CDW}}$. The electronic dispersion $E(\mathbf{q}) = \pm\sqrt{|\hbar v_F \mathbf{q}|^2 + m_{\mathrm{CDW}}^2}$ then exhibits an energy gap $2|m_{\mathrm{CDW}}|$. This state describes an ordinary insulator.

Haldane imagined lifting the degeneracy by breaking time reversal symmetry. This can be done by applying a magnetic field that is zero on the average, but has all of the spatial symmetries of the honeycomb lattice. This can be represented by an imaginary second neighbor hopping term, which has a sign that depends on whether the electron makes a left or right turn going from the first to second neighbor. This leads to

$$d_z^H(\mathbf{k}) = \lambda_H \sum_{p<p'=1}^{3} s_{pp'} \sin \mathbf{k} \cdot (\mathbf{a}_p - \mathbf{a}_{p'}), \tag{29}$$

with $s_{pp'} = \pm 1$ when $p' = p \pm 1 \bmod 3$. This also introduces a mass to the Dirac points. Since $d_z(-\mathbf{k}) = -d_z(\mathbf{k})$, the masses at $\mathbf{K}$ and $\mathbf{K}'$ have *opposite* sign, so that in the continuum theory,

$$\Delta\mathcal{H}^H = m_H \sigma^z \tau^z \tag{30}$$

with $m_H = 3\sqrt{3}\lambda_H$. Haldane showed that this gapped state is not an ordinary insulator, but rather has a quantized Hall conductivity $\sigma_{xy} = e^2/h$.

The Hall conductivity can be understood by considering the Chern number for the two band model in terms of (8). When the $m_{\mathrm{CDW}} = m_H = 0$, $\hat{\mathbf{d}}(\mathbf{k})$ is confined to the equator $d_z = 0$, with a unit (and opposite) winding around each of the Dirac points where $|\mathbf{d}| = 0$. For $m_{\mathrm{CDW}} > m_H$, $|\mathbf{d}|$ is nonzero everywhere, and visits the north pole near both $\mathbf{K}$ and $\mathbf{K}'$. The net solid angle subtended is thus zero, and $\sigma_{xy} = 0$. For $m_H > m_{\mathrm{CDW}}$ the masses at $\mathbf{K}$ and $\mathbf{K}'$ have opposite sign, so that $\hat{\mathbf{d}}(\mathbf{k})$ visits both the north and the south pole, and wraps the sphere once. Thus $\sigma_{xy} = e^2/h$. For $m_{\mathrm{CDW}} = m_H$, $d_z(\mathbf{K}) = 0$, so that the system is at a gapless quantum critical point characterized by a single 2D massless Dirac fermion.

4.3 Chiral Edge States, and the Bulk Boundary Correspondence

A fundamental consequence of the topological classification of gapped band structures is the existence of gapless conducting states at interfaces where the topological invariant changes. Such edge states are well known at the interface between the integer quantum Hall state and vacuum [14]. They may be understood in terms of the semiclassical skipping orbits that electrons undergo as their cyclotron orbits bounce off the edge (Fig. 9(a)). Importantly, the electronic states responsible for this motion are *chiral* in the sense that they propagate in one direction only along the edge. These states are insensitive to disorder because there are no states available for backscattering—a fact that underlies the perfectly quantized electronic transport in the quantum Hall effect. The existence of such "one way" edge states is deeply related to the topology of the bulk quantum Hall state.

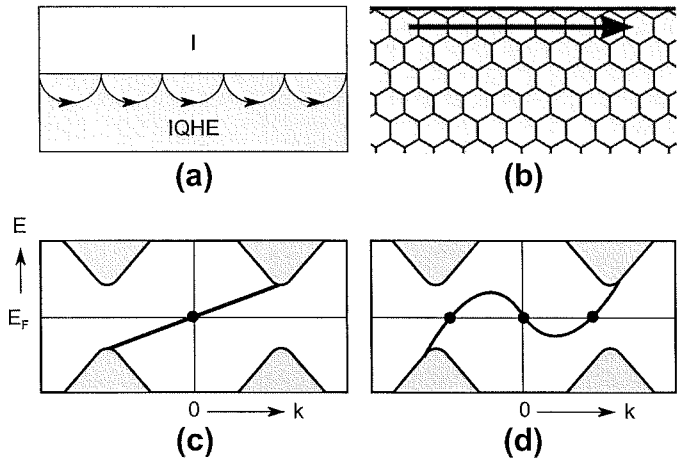

FIGURE 9 (a) Edge states as skipping cyclotron orbits. (b) Edge states in Haldane's model on a semi-infinite plane. (c) The chiral edge states connect the valence band near **K** and **K**′. (d) By changing the Hamiltonian near the edge, the details of the edge states change, but $N_R - N_L = 1$ remains fixed.

A simple theory of the chiral edge states can be developed using the two band Dirac model (28). Consider an interface where the mass m at one of the Dirac points changes sign as a function of y. We thus let $m \to m(y)$, where $m(y) > 0$ gives the insulator for $y > 0$ and $m(y) < 0$ gives the quantum Hall state for $y < 0$. Assume $m' > 0$ is fixed. Translation symmetry in the x direction allows us to consider plane wave states $\psi_{q_x}(x,y) = e^{iq_x x}\phi(y)$. For each q_x, the problem is identical to the Jackiw Rebbi problem discussed in Section 3.3. The zero energy mode $\phi_0(y)$ has precisely the form of (20), and leads to a band with dispersion

$$E(q_x) = \hbar v_F q_x. \tag{31}$$

This band of states intersects the Fermi energy E_F with a positive group velocity $dE/dq_x = \hbar v_F$ and defines a right moving chiral edge mode.

The chiral edge states can also be seen explicitly by solving the Haldane model in a semi-infinite geometry with an edge at $y = 0$ (Fig. 9(b)). Figure 9(c) shows the energy levels as a function of the momentum k_x along the edge. The solid regions show the bulk conduction and valence bands, which form continuum states and show the energy gap near **K** and **K**′. A single band, describing states bound to the edge, connects the valence band at **K**′ to the conduction band at **K** with a positive group velocity.

By changing the Hamiltonian near the surface the precise dispersion of the edge states can be modified. For instance, $E(q_x)$ could develop a kink so that the edge states intersect the Fermi energy three times—twice with a positive group velocity and once with a negative group velocity, as in Fig. 9(d). The difference $N_R - N_L$ between the number of right moving and left moving modes,

however, cannot change, and is an integer topological invariant characterizing the interface. The value of $N_R - N_L$ is determined by the topological structure of the bulk states. This is summarized by the *bulk-boundary correspondence*:

$$N_R - N_L = \Delta n, \tag{32}$$

where Δn is the difference in the Chern number across the interface.

5 $\mathbb{Z}_2$ TOPOLOGICAL INSULATORS

Since the Hall conductivity (and hence the TKNN invariant) is odd under time reversal, the topologically nontrivial states described in the preceding section can only occur when time reversal symmetry is broken either by an external magnetic field or by magnetic order. However, the spin orbit interaction allows a *different* topological class of insulating band structures when time reversal symmetry is unbroken [4]. In this section we will introduce the $\mathbb{Z}_2$ topological insulators and show that they exhibit protected boundary states.

The possibility of a time reversal invariant 2D topological insulator was first noticed in a model of graphene with spin orbit interactions [3]. We will begin by introducing that model of a quantum spin Hall insulator, from which it is straightforward to establish the existence of edge states, and to see why they are protected. We will then go onto consider the quantum spin Hall insulator in more generality and show that it is protected by a $\mathbb{Z}_2$ topological invariant. We will discuss how the $\mathbb{Z}_2$ invariant can be computed, as well as its consequences. Finally, we will briefly introduce the three-dimensional topological insulators, which will be discussed in detail in the following chapter.

5.1 Quantum Spin Hall Insulator in Graphene

In Section 4.2 we argued that the degeneracy at the Dirac point in graphene is protected by inversion and time reversal symmetry. However, that argument ignored the spin of the electrons. The spin orbit interaction allows a new mass term in (26) that leads to a topological insulating state [3].

That such a mass term is possible can be easily understood by considering the symmetries of the possible mass terms. Without spin, it is clear that the only possible terms in (26) that can open a gap are $\lambda_{\text{CDW}}\sigma^z$ (which violates inversion) and $\lambda_H\sigma^z\tau^z$ (which violates time reversal). The spin degree of freedom allows a new mass term of the form

$$\delta\mathcal{H}^{\text{SO}} = \lambda_{\text{SO}}\sigma^z\tau^z s^z, \tag{33}$$

where $s^z = \pm 1$ represents the spin degree of freedom. This term respects all of the symmetries of graphene, so it must be present. However, since the spin orbit interaction in carbon is weak, this term is small, and has not yet been observed. Nonetheless, it is of conceptual value to consider its effects.

Taken separately, the Hamiltonians for the $s_z = \pm 1$ spins violate time reversal symmetry and are equivalent to Haldane's model for spinless electrons, which gives quantized Hall conductivity $\pm e^2/h$. An applied electric field thus leads to Hall currents for the $s_z = \pm 1$ spins that cancel each other, but generate a net spin current $\mathbf{J}_s = (\hbar/2e)(\mathbf{J}_\uparrow - \mathbf{J}_\downarrow)$ characterized by a quantized spin Hall conductivity $\sigma^s_{xy} = e/2\pi$. This is the origin of the name "quantum spin Hall effect." However, it must be emphasized that this quantized spin Hall conductivity is an artifact of an oversimplified model in which the spin s^z is conserved. In reality, spin is not conserved, and this quantization will break down in the presence of s^z nonconserving interactions.

Since it is two copies of a quantum Hall state, the quantum spin Hall state must have gapless edge states. Unlike the quantized Hall conductivity, these edge states remain robust even when spin is not conserved. These edge states have the special "spin filtered" property that up and down spins propagate in opposite directions. They were later dubbed "helical," in analogy with the correlation between spin and momentum of a particle known as helicity [41]. They form a unique 1D conductor that is essentially half of an ordinary 1D conductor. Ordinary conductors, which have up and down spins propagating in both directions, are fragile because the electronic states are susceptible to Anderson localization in the presence of weak disorder. By contrast, the quantum spin Hall edge states cannot be localized even for strong disorder. Here we will present one argument that this is the case [3]. Another proof will be given in Section 5.2.2.

Imagine an edge that is disordered in a finite region and perfectly clean outside that region. The exact eigenstates can be determined by solving the scattering problem relating incoming waves to those reflected from and transmitted through the disordered region. They will be characterized by a 2×2 unitary S matrix, which relates the incoming to outgoing states, $\Phi_{\text{out}} = S\Phi_{\text{in}}$, where Φ is a two component spinor consisting of the left and right moving edge states $\phi_{L\uparrow}$ and $\phi_{R\downarrow}$. Time reversal symmetry (to be discussed in more detail below) relates the left and right moving states by $\Phi_{\text{in,out}} \rightarrow \sigma^y \Phi^*_{\text{out,in}}$. Time reversal therefore imposes a constraint on the S matrix of the form $S = \sigma^y S^T \sigma^y$. It is straightforward to show that this requires the off diagonal component of S, which describes backscattering, to vanish. It follows that unless time reversal symmetry is broken, an incident electron is transmitted perfectly across the disordered region. Thus, eigenstates at any energy are extended, and at temperature $T = 0$ the edge state transport is ballistic. For $T > 0$ inelastic backscattering processes are allowed, which will, in general, lead to a finite conductivity.

The edge states can be explicitly seen in a lattice model that generalizes Haldane's model to include the intrinsic symmetry-allowed spin orbit interaction. We thus add to (26) a second neighbor spin dependent hopping amplitude proportional to $i\vec{s} \cdot (\mathbf{a}_1 \times \mathbf{a}_2)$, where $\mathbf{a}_{1,2}$ are the nearest neighbor bonds traversed. Such a term does not break any symmetries of the graphene

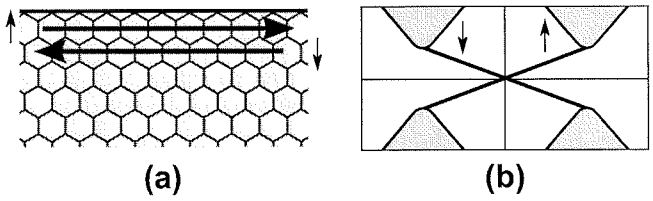

FIGURE 10 The edge states in graphene with the intrinsic spin orbit interaction have the spin filtered property that up and down spins propagate in opposite directions.

lattice, and can be represented as

$$\Delta H^{\mathrm{SO}}(\mathbf{k}) = \lambda_{\mathrm{SO}} s^z \vec{\sigma} \cdot \mathbf{d}^H(\mathbf{k}), \tag{34}$$

where $\mathbf{d}^H$ is given in (29). The resulting theory is simply two time reversed copies of Haldane's model, and on a semiinfinite strip has a spectrum shown in Fig. 10.

5.2 $\mathbb{Z}_2$ Topological Invariant

The fact that the edge states of the quantum spin Hall insulator are robust suggests that there must be a topological distinction between the quantum spin Hall insulator and an ordinary insulator. In this section we describe that topological invariant [4,42]. We will begin with a discussion of time reversal symmetry. We will then argue using the bulk-boundary correspondence that there are two and only two topological classes of time reversal invariant band structures. We will then discuss the physical meaning of the $\mathbb{Z}_2$ invariant as well as how to determine it.

5.2.1 Time Reversal Symmetry

The key to understanding this new topological class is to examine the role of $\mathcal{T}$ symmetry for spin 1/2 particles. $\mathcal{T}$ symmetry is represented by an antiunitary operator $\Theta = \exp(i\pi S_y/\hbar)K$, where S_y is the spin operator and K is complex conjugation. For spin 1/2 electrons, Θ has the property $\Theta^2 = -1$. This leads to an important constraint, known as Kramers' theorem, that all eigenstates of a $\mathcal{T}$ invariant Hamiltonian are at least twofold degenerate. This follows because if a nondegenerate state $|\chi\rangle$ existed then $\Theta|\chi\rangle = c|\chi\rangle$ for some constant c. This would mean $\Theta^2|\chi\rangle = |c|^2|\chi\rangle$, which is not allowed because $|c|^2 \neq -1$. In the absence of spin orbit interactions, Kramers' degeneracy is simply the degeneracy between up and down spins. In the presence of spin orbit interactions, however, it has nontrivial consequences.

A $\mathcal{T}$ invariant Bloch Hamiltonian must satisfy

$$\Theta \mathcal{H}(\mathbf{k}) \Theta^{-1} = \mathcal{H}(-\mathbf{k}). \tag{35}$$

One can classify the equivalence classes of Hamiltonians satisfying this constraint that can be smoothly deformed without closing the energy gap. The TKNN invariant is $n = 0$, but there is an additional invariant with two possible values $\nu = 0$ or 1 [4]. The fact that there are two and only two topological classes can be understood by appealing to the bulk-boundary correspondence.

5.2.2 Bulk Boundary Correspondence

In Fig. 11 we show plots analogous to Fig. 10(b) showing the electronic states associated with the edge of a $\mathcal{T}$ invariant 2D insulator as a function of the crystal momentum along the edge. Only half of the Brillouin zone $\Gamma_a = 0 < k_x < \Gamma_b = \pi/a$ is shown because $\mathcal{T}$ symmetry requires that the other half $-\pi/a < k < 0$ is a mirror image. As in Fig. 10(b), the shaded regions depict the bulk conduction and valence bands separated by an energy gap. Depending on the details of the Hamiltonian near the edge there may or may not be states bound to the edge inside the gap. If they are present, however, then Kramers' theorem requires they be twofold degenerate at the $\mathcal{T}$ invariant momenta $k_x = 0$ and $k_x = \pi/a$ (which is the same as $-\pi/a$). Away from these special points, labeled $\Gamma_{a,b}$ in Fig. 11, a spin orbit interaction will split the degeneracy. There are two ways the states at $k_x = 0$ and $k_x = \pi/a$ can connect. In Fig. 11(a) they connect pairwise. In this case the edge states can be eliminated by pushing all of the bound states out of the gap. Between $k_x = 0$ and $k_x = \pi/a$, the bands intersect E_F an even number of times. In contrast, in Fig. 11(b) the edge states cannot be eliminated. The bands intersect E_F an odd number of times.

Which of these alternatives occurs depends on the topological class of the bulk band structure. Since each band intersecting E_F at k_x has a Kramers partner at $-k_x$, the bulk-boundary correspondence relates the number N_K of Kramers pairs of edge modes intersecting E_F to the change in the $\mathbb{Z}_2$ invariants across the interface,

$$N_K = \Delta\nu \bmod 2. \tag{36}$$

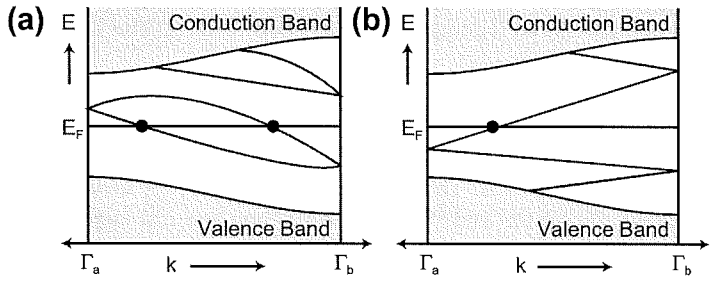

FIGURE 11 Electronic dispersion between two boundary Kramers degenerate points. In (a) the number of surface states crossing the Fermi energy E_F is even, whereas in (b) it is odd. An odd number of crossings leads to topologically protected metallic boundary states.

We conclude that a 2D topological insulator has topologically protected edge states. 3D topological insulators, discussed in Section 5.3, have protected surface states.

As discussed in Section 5.1, the edge states form a unique 1D conductor, which cannot be localized, even for strong disorder. Figure 11 provides a simple way of seeing why this must be the case [42]. Consider a cylinder with a large diameter, but treat the entire circumference as a single very large unit cell $a = 2\pi R$. Then the role of the momentum in Fig. 11 is played by the magnetic flux threading the cylinder, which gives a phase for the periodic boundary condition. Flux $\Phi = 0$ corresponds to $k = 0$, while $\Phi = \phi_0/2$ corresponds to $k = \pi/a$. In a clean system there will be many level crossings for $0 < k < \pi/a$ because the Brillouin zone has been folded back many times. However, in the presence of disorder all accidental degeneracies will be lifted. It is clear that when the unit cell is doubled and accidental degeneracies are removed, the folded Brillouin zone will keep its structure described in Fig. 11(a) and (b). Thus, for a topological insulator cylinder with $a = 2\pi R$, the spectrum "switches partners" as a function of magnetic flux. The spectrum is thus sensitive to the boundary conditions around the cylinder. This proves that every eigenstate must be extended, because localized states are insensitive to boundary conditions.

5.2.3 *Physical Meaning of the Invariant*

In Section 3.1, we interpreted the Chern number characterizing the integer quantum Hall effect in terms of Laughlin's argument and a 1D Thouless charge pump. The Chern number describes the change in the electric polarization when flux $\Phi = \phi_0$ is adiabatically threaded through the cylinder. An equivalent formulation is to deform the cylinder into a Corbino disk with a small hole threaded by flux. Laughlin's argument [33] then describes the binding of electric charge to the flux threading the hole. It is clear that this formulation is more general than the noninteracting electron framework that we have been using. The Laughlin argument can equally be applied to an interacting system, since the change in polarization is well defined in a many body setting. The $\mathbb{Z}_2$ invariant can be understood similarly [42].

Consider again a cylinder with a finite radius, so that the eigenstates associated with the ends are discrete. When this system is viewed as a 1D system, we wish to ask whether there is a Kramers degeneracy in the ground state associated with the ends. This would be the case if, for instance, there was an unpaired spin at the end. When there is time reversal symmetry, the existence of a Kramers degeneracy is a yes/no question. It is determined by whether the number of electrons is locally even or odd. We refer to this $\mathbb{Z}_2$ quantity as the "time reversal polarization," or the "local fermion parity." Like the polarization in Laughlin's argument, the time reversal polarization can be defined in an interacting system.

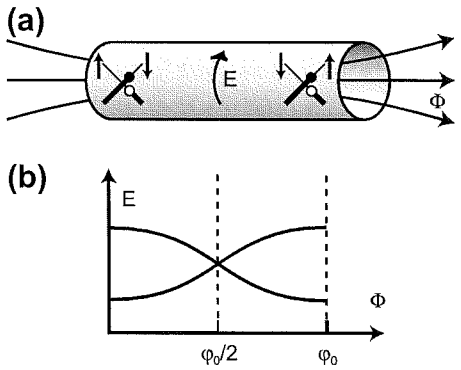

FIGURE 12 (a) When flux $\phi_0/2$ is threaded through a cylinder, the "time reversal polarization changes." (b) shows the evolution of the many body energy levels as a function of flux. When $\Phi = \phi_0/2$ the ground state is Kramers degenerate.

The $\mathbb{Z}_2$ topological invariant characterizes the *change* in the time reversal polarization when the flux Φ is changed from 0 to $\phi_0/2$. In the spin conserving case, the change in the Kramers degeneracy is easy to see because the $\phi_0/2$ flux insertion transfers "half" a spin up to the left and "half" a spin down to the right. Thus the eigenvalue of S_z associated with the end changes by $\hbar/2$, and due to Kramers' theorem, the degeneracy changes. Relaxing the S_z conservation (while preserving time reversal) prevents us from labeling the states with S_z, but the change in time reversal polarization remains well defined. The presence of Kramers degeneracy depends on whether the number of electrons is locally even or odd. Threading flux $\phi_0/2$ through the cylinder acts as a "pump" for fermion parity.

It is instructive to compare this interpretation with the edge state pictures in Fig. 11. If we view the cylinder as consisting of a single large unit cell in the azimuthal direction, then Fig. 11 describes the discrete end state spectrum as a function of flux, with $k = \Gamma_a = 0$ corresponding to $\Phi = 0$ and $k = \Gamma_b = \pi/a$ corresponding to $\Phi = \phi_0/2$. Suppose at $\Phi = 0$ there are no partially occupied Kramers pairs, so that the many body ground state is nondegenerate. Then at $\Phi = \phi_0$ there will be a single half-filled Kramers pair, which gives a Kramers degenerate many body state, when the $\mathbb{Z}_2$ invariant is nontrivial (see Fig. 12).

If we flatten the cylinder into a Corbino disk, then a flux $\phi_0/2$ piercing a topological insulator is associated with an odd fermion parity, but no net charge. This is an example of fractionalization, where the spin and charge of the electron decouple.

5.2.4 Formulas for the $\mathbb{Z}_2$ Invariant

There are several mathematical formulations of the $\mathbb{Z}_2$ invariant [4,7,10,42–47] ν. One approach [42] is to define a unitary matrix

$$w_{mn}(\mathbf{k}) = \langle u_m(\mathbf{k})|\Theta|u_n(-\mathbf{k})\rangle \tag{37}$$

built from the occupied Bloch functions $|u_m(\mathbf{k})\rangle$. Since Θ is anti-unitary and $\Theta^2 = -1, w^T(\mathbf{k}) = -w(-\mathbf{k})$. There are four special points Λ_a in the bulk 2D Brillouin zone where $\mathbf{k}$ and $-\mathbf{k}$ coincide, so $w(\Lambda_a)$ is antisymmetric. The determinant of an antisymmetric matrix is the square of its pfaffian, which allows us to define

$$\delta_a = \mathrm{Pf}[w(\Lambda_a)]/\sqrt{\mathrm{Det}[w(\Lambda_a)]} = \pm 1. \tag{38}$$

Provided $|u_m(\mathbf{k})\rangle$ is chosen continuously throughout the Brillouin zone (which is always possible), the branch of the square root can be specified globally, and the $\mathbb{Z}_2$ invariant is

$$(-1)^\nu = \prod_{a=1}^{4} \delta_a. \tag{39}$$

This formulation can be generalized to 3D topological insulators, and involves the eight special points in the 3D Brillouin zone.

The calculation of ν is considerably simpler if the crystal has extra symmetry. For instance, if the 2D system conserves the perpendicular spin S_z, then the up and down spins have independent Chern integers $n_\uparrow, n_\downarrow$. $\mathcal{T}$ symmetry requires $n_\uparrow + n_\downarrow = 0$, but the difference $n_\sigma = (n_\uparrow - n_\downarrow)/2$ defines a quantized spin Hall conductivity [52]. The $\mathbb{Z}_2$ invariant is then simply

$$\nu = n_\sigma \bmod 2. \tag{40}$$

While $n_\uparrow, n_\downarrow$ lose their meaning when S_z nonconserving terms (which are inevitably present) are added, ν retains its identity.

If the crystal has inversion symmetry there is another shortcut [10] to computing ν. At the special points Λ_a the Bloch states $u_m(\Lambda_a)$ are also parity eigenstates with eigenvalue $\xi_m(\Lambda_a) = \pm 1$. The $\mathbb{Z}_2$ invariant then simply follows from (39) with

$$\delta_a = \prod_m \xi_m(\Lambda_a), \tag{41}$$

where the product is over the Kramers pairs of occupied bands. This has proven useful for identifying topological insulators from band structure calculations [10,48–51].

For crystals without inversion symmetry determining the $\mathbb{Z}_2$ invariant is more difficult to implement numerically because (39) requires a continuous gauge, which is not provided by the computer. Efficient algorithms for numerically computing the $\mathbb{Z}_2$ invariant numerically have, however, been developed [53].

5.3 Topological Insulators in Three Dimensions

3D topological insulators will be discussed in detail in the following chapter. Here we will discuss them briefly in a manner that makes contact with our

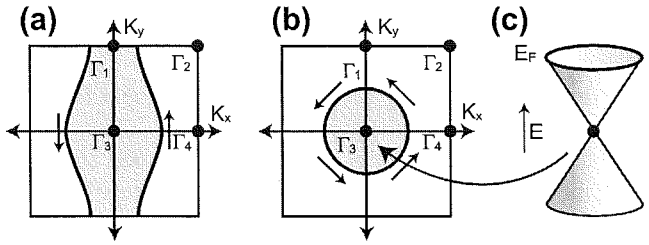

FIGURE 13 Fermi circles in the surface Brillouin zone for (a) a weak topological insulator and (b) a strong topological insulator. (c) In the simplest strong topological insulator the Fermi circle encloses a single Dirac point.

discussion of the quantum spin Hall insulator. A 3D topological insulator is characterized by four $\mathbb{Z}_2$ topological invariants $(\nu_0; \nu_1\nu_2\nu_3)$ [7–9]. They can be most easily understood by appealing to the bulk-boundary correspondence, discussed in Section 5.2.2. The surface states of a 3D crystal can be labeled with a 2D crystal momentum. There are four $\mathcal{T}$ invariant points $\Gamma_{1,2,3,4}$ in the surface Brillouin zone, where surface states, if present, must be Kramers degenerate (Fig. 13(a,b)). Away from these special points, the spin orbit interaction will lift the degeneracy. These Kramers degenerate points therefore form 2D *Dirac points* in the surface band structure (Fig. 13(c)). The interesting question is how the Dirac points at the different $\mathcal{T}$ invariant points connect to each other. Between any pair Γ_a and Γ_b, the surface state structure will resemble either Fig. 11(a) or (b). This determines whether the surface Fermi surface intersects a line joining Γ_a to Γ_b an even or an odd number of times. If it is odd, then the surface states are topologically protected. Which of these two alternatives occurs is determined by the four bulk $\mathbb{Z}_2$ invariants.

5.3.1 Weak Topological Insulator

The simplest nontrivial 3D topological insulators may be constructed by stacking layers of the 2D quantum spin Hall insulator. This is analogous to a similar construction for 3D integer quantum Hall states [54]. Consider a stack of weakly coupled layers of $\nu = n$ integer quantum Hall states. Each layer will have Hall conductivity e^2/h, leading to a 3D conductivity tensor,

$$\sigma_{\mu\nu} = \frac{e^2}{2\pi h}\epsilon_{\mu\nu\lambda}\mathbf{G}_\lambda, \tag{42}$$

where $\mathbf{G} = (2\pi/d)n\hat{\mathbf{n}}$ is a reciprocal lattice vector associated with the layers with separation d perpendicular to $\hat{\mathbf{n}}$. The edge states on each layer will form a chiral surface sheath. It is clear that when coupling between the layers is introduced the Hall conductivity and the surface states will remain, provided the bulk gap remains finite. The reciprocal lattice vector $\mathbf{G}$ is then specified by

three integer Chern numbers, which characterize the three independent planes in momentum space.

Consider now a stack of weakly coupled 2D quantum spin Hall insulator layers. The helical edge states of the layers now become anisotropic surface states. A possible surface Fermi surface for weakly coupled layers stacked along the y direction is sketched in Fig. 13(a). In this figure a single surface band intersects the Fermi energy between Γ_1 and Γ_2 and between Γ_3 and Γ_4, leading to the nontrivial connectivity in Fig. 11(b). This layered state is referred to as a weak topological insulator, and has $\nu_0 = 0$. The indices $(\nu_1\nu_2\nu_3)$ can be interpreted as Miller indices describing the "mod 2" reciprocal lattice vector

$$\mathbf{G}^{\nu} = \nu_1\mathbf{b}_1 + \nu_2\mathbf{b}_2 + \nu_3\mathbf{b}_3. \tag{43}$$

Here $\mathbf{b}_i$ are primitive reciprocal lattice vectors, and $\mathbf{G}^{\nu}$, which characterizes the layers, is defined modulo twice a reciprocal lattice vector.

Unlike the 2D helical edge states of a single layer, $\mathcal{T}$ symmetry does not protect these surface states. Though the surface states must be present for a clean surface, by breaking the translational symmetry, it is possible to eliminate the surface states without closing the bulk gap. The simplest way to see this is to imagine adding a dimerization (analogous to the SSH model, Fig. 4), which strongly couples pairs of layers, which results in a stack of trivial insulators.

Interestingly, however, there remain robust topological features associated with weak topological insulators. A line *dislocation* in a weak topological insulator is associated with protected 1D helical edge states [55]. This is easy to understand for weakly coupled layers in the case of an edge dislocation, where the dislocation involves a layer that ends on the dislocation line, and is associated with a helical edge state. Clearly, when the coupling between the layers is increased the edge state cannot disappear.

In addition, there has been interesting recent work characterizing the surface states of weak topological insulators in the presence of disorder [56–58]. The key point is that opening a gap by dimerization requires breaking the discrete lattice translation symmetry, which is not expected to occur in a macroscopic system. The surface of a weak topological insulator is thus expected to remain metallic, even for strong disorder.

5.3.2 Strong Topological Insulator

$\nu_0 = 1$ identifies a distinct phase, called a strong topological insulator, which cannot be interpreted as a descendant of the 2D quantum spin Hall insulator. ν_0 determines whether an even or an odd number of Kramers points is enclosed by the surface Fermi circle. In a strong topological insulator the surface Fermi circle encloses an *odd* number of Kramers degenerate Dirac points. The simplest case, with a single Dirac point (Fig. 13(b,c)), can be described by the Hamiltonian,

$$\mathcal{H}_{\text{surface}} = -i\hbar v_F \vec{\sigma} \cdot \vec{\nabla}, \tag{44}$$

where $\vec{\sigma}$ characterizes the spin. (For a surface with a mirror plane, symmetry requires $\vec{S} \propto \hat{z} \times \vec{\sigma}$.) The surface electronic structure of a topological insulator is similar to graphene, except rather than having four Dirac points (2 valley $\times$ 2 spin) there is just a single Dirac point.

The surface states of a strong topological insulator form a unique 2D topological metal [9,10] that is essentially *half* an ordinary metal. Unlike an ordinary metal, which has up and down spins at every point on the Fermi surface, the surface states are not spin degenerate. Since $\mathcal{T}$ symmetry requires that states at momenta $\mathbf{k}$ and $-\mathbf{k}$ have opposite spin, the spin must rotate with $\mathbf{k}$ around the Fermi surface, as indicated in Fig. 13(b). This leads to a nontrivial Berry phase acquired by an electron going around the Fermi circle. $\mathcal{T}$ symmetry requires that this phase be 0 or π. When an electron circles a Dirac point, its spin rotates by 2π, which leads to a π Berry phase.

The Berry phase has important consequences for the behavior in a magnetic field and for the effects of disorder. In particular, in an ordinary 2D electron gas the electrical conductivity decreases with decreasing temperature, reflecting the tendency toward Anderson localization in the presence of disorder [59]. The π Berry phase changes the sign of the weak localization correction to the conductivity leading to weak *antilocalization* [60].

In fact, the electrons at the surface of a strong topological insulator cannot be localized even for strong disorder, as long as the bulk energy gap remains intact. The argument at the end of Section 5.2.2 can easily be generalized to 3D [61]. Consider a 3D topological insulator with periodic boundary conditions in two directions, but open boundary conditions in the third direction. This has the topology of a thickened torus with inside and outside surfaces, which was called a "Corbino doughnut" in Ref. [10], in analogy with the Corbino disk. There are now two independent fluxes associated with the two periodic directions, and the system has time reversal symmetry if these fluxes are either 0 or $\phi_0/2$. If we view the entire surface as a single unit cell, then the fluxes play the role of the two components of momentum in Fig. 13(b). This leads to sensitivity to boundary conditions described by Fig. 11. For the strong topological insulator, the odd number of crossings depicted in Fig. 13(b) persists when the unit cell is doubled. Therefore, the surface states of the topological insulator must be sensitive to the periodic boundary conditions, so they can not be localized.

6 RELATED TOPICS

We close by briefly mentioning some further applications of topological band theory. Some of these topics will be discussed in detail in later chapters.

6.1 Topological Crystalline Insulators

Spatial symmetries can modify and enhance the topological structure of band theory. The simplest example of this occurred in the SSH model, discussed in

Section 3.2, where the presence of inversion symmetry led to the topological distinction between the two dimerization patterns, which in the absence of inversion symmetry are topologically equivalent. A second example is the weak topological insulator, where translation symmetry plays an essential role. This leads to a broader class of topological band structures that are "less topological" than topological insulators (because disorder breaks all spatial symmetries), but nonetheless lead to interesting consequences.

A completely general classification of band structures with space group symmetries is a challenging math problem. Most progress to date has focused on specific examples. One class of topological invariants, which can exist when a system has mirror symmetry, is the "mirror Chern number" [48,62,63]. Consider the graphene model discussed in Section 5.1. This model has a mirror symmetry under $z \to -z$. It follows that eigenstates can be labeled with eigenvalues of that mirror operation. Importantly, since a mirror can be expressed as inversion times a 180° rotation, the eigenvalues of the mirror operator for spin 1/2 particles are $\pm i$, which means that the mirror operator is odd under time reversal. It is therefore possible to define Chern numbers $n_{\pm i}$ for the states with mirror eigenvalue $\pm i$. Time reversal symmetry dictates that $n_{+i} + n_{-i} = 0$, but the difference $n^M = (n_{+i} - n_{-i})/2$ defines a crystal symmetry protected integer topological invariant. For graphene, the $\mathbb{Z}_2$ invariant is simply $(-1)^{n^M}$.

The mirror Chern number can also be applied to 3D insulators [48,62,63]. In this case, mirror invariant planes in momentum space can be characterized by a mirror Chern number. This leads to consequences for the structure of the surface states. On surfaces that are perpendicular to a mirror plane (so that the surface retains the mirror symmetry) the surface must have gapless modes. A gap can be opened, however, if the mirror symmetry is broken. The situation is quite similar to a weak topological insulator, where the gapless surface states are protected by a discrete translation symmetry. In both cases, if disorder breaks the symmetry locally, but the symmetry is not macroscopically broken, then one expects the surface to remain conducting even in the presence of disorder. This is an interesting situation that warrants further exploration.

6.2 Topological Nodal Semimetals

Materials that are not insulators can also have topological aspects to their band structure [24]. One case of interest are nodal semimetals [64–66], in which the conduction band and valence band touch each other at points, leading to a Dirac-type low energy electronic structure. In 3D, the point touching of two nondegenerate bands, known as a Weyl point, is topologically protected. This is easy to understand by expanding the Hamiltonian around the degeneracy point. To linear order, for suitable coordinates k_i, the Hamiltonian can be written $H(\mathbf{k}) = v_{ij}\sigma_i k_j$. Importantly, in 3D, all three Pauli matrices are used, so that any perturbation, which may be written $u_0 I + \vec{u} \cdot \vec{\sigma}$, will only shift the location

of the Weyl point and cannot open a gap. This topological protection can also be understood in terms of the Chern number $n = \text{sgn}(\det[v_{ij}])$ characterizing $H(\mathbf{k})$ on a sphere surrounding the Weyl point.

Time reversal symmetry requires Weyl points to come in pairs at $\pm\mathbf{K}$, with opposite Chern numbers, while inversion symmetry requires pairs at $\pm\mathbf{K}$ with the same Chern number. Thus, the presence of isolated Weyl points in a band structure requires breaking time reversal and/or inversion symmetry. The time reversal broken state exhibits an interesting anomalous Hall conductivity. In both cases, the surface exhibits interesting Fermi arcs that terminate on the projected Weyl points. Candidate materials and structures for Weyl semimetals have been proposed [64–66]. It will be interesting to observed these effects experimentally.

It is also possible to have nodal semimetals that are protected by point group symmetries. Dirac semimetals have fourfold degenerate band crossings at the Fermi level [67]. These are not topologically protected in the way Weyl points are, but can be protected by crystal symmetries which enforce the degeneracy. Such Dirac points occurred in a model system based on a diamond lattice, and candidate materials have been proposed.

6.3 Topological Superconductivity

Topological superconductivity is a beautiful subject that will be treated in detail elsewhere. Here we will just mention that considerations of topological band theory can also be used to classify superconductors. The Bardeen, Cooper, and Schrieffer (BCS) mean field theory of superconductivity is a noninteracting theory, which in addition to the usual terms includes anomalous terms of the form $\Delta\psi^\dagger\psi^\dagger$. These can be analyzed in terms of a one body Hamiltonian if the one body Hilbert space is artificially doubled to include both positive and negative energy states. This results in a Bloch-Bogoliubov de Gennes Hamiltonian $H(\mathbf{k})$ that is just like a Bloch Hamiltonian, except that it has an intrinsic particle-hole symmetry

$$H(\mathbf{k}) = -\Xi H(-\mathbf{k})\Xi^{-1}, \tag{45}$$

where Ξ is an antiunitary operator. This has a structure similar to time reversal symmetry in Eq. (35). Like time reversal symmetry it modifies the topological classifications of gapped Hamiltonians, leading to classes of topological superconductors. The bulk-boundary correspondence in topological superconductors leads to topologically protected boundary modes. The redundancy that was introduced by doubling the one body Hilbert space makes these boundary modes Majorana fermion modes.

Allowing for both time reversal and particle-hole symmetry leads to an elegant generalization of topological band theory [24,68–71]. There are 10 symmetry classes, which depend on the presence or absence of $\mathcal{T}$ symmetry

(with $\Theta^2 = \pm 1$) and/or particle-hole symmetry (with $\Xi^2 = \pm 1$). The topological classifications, given by $\mathbb{Z}$, $\mathbb{Z}_2$, or 0, show a regular pattern as a function of symmetry class and dimensionality, dubbed the "10-fold way."

6.4 Topological Defects

Finally, we note that topological band theory can classify and characterize topological defects that carry protected gapless modes [72]. Let us illustrate this with a simple example. Consider a three-dimensional quantum Hall state, which can be viewed as a stack of layers of 2D quantum Hall states. For simplicity first consider the weakly coupled limit where the layers are independent. Consider now an edge dislocation, shown in Fig. 14, which occurs when one of the layers is terminated along a line. It is clear that line will be associated with a chiral edge state. Now imagine that coupling between the layers is turned on, but the bulk gap remains finite. The chiral edge state has nowhere to go and must remain. Its presence is guaranteed topologically in the same way the edge states in the 2D quantum Hall effect are guaranteed.

We thus have a topologically protected "boundary mode." For the 3D structure, what is the analog of the bulk? To analyze this it is useful to consider a large circle surrounding the dislocation line in real space. Far away from the dislocation the Hamiltonian varies slowly with position s along the circle. We thus have a one parameter *family* of bandstructures $H(\mathbf{k}, s)$, where s is defined on the circle. A circle that encloses a chiral edge state must be topologically distinct from a circle that does not enclose a chiral edge state. We are thus led to topologically classify *families* of gapped bandstructures $H(\mathbf{k}, s)$. Such a four parameter family of Hamiltonians is classified by an integer topological invariant called the second Chern number. In the layered quantum Hall state the second Chern number can be computed [72] and is given by $n = \mathbf{G} \cdot \mathbf{B}/2\pi$,

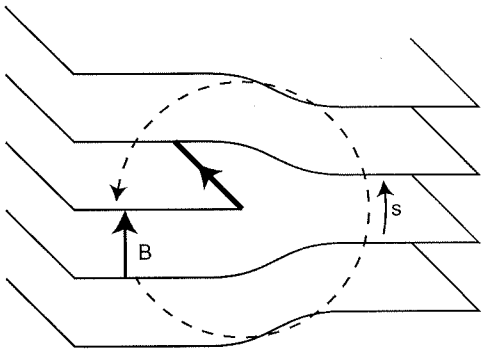

FIGURE 14 A dislocation line, with Burgers vector **B** in a layered 3D quantum Hall state, is associated with a gapless 1D chiral fermion mode.

where **B** is the Burgers vector characterizing the dislocation and **G**, defined in (42), characterizes the quantum Hall state.

It is clear that this method of analysis is more general than this specific example. For example, a similar analysis explains the helical modes associated with a dislocation in a weak topological insulator. The analysis of D parameter families of Hamiltonians in d dimensions ($H(\mathbf{k},\mathbf{r})$ with $\mathbf{k} \in T^d$ and $\mathbf{r} \in S^d$) with or without time reversal symmetry leads to a generalization of the bulk-boundary correspondence that applies generally to the protected modes associated with $d - D - 1$ dimensional topological defects. When combined with the theory of topological superconductivity it leads to a generalization of the "ten-fold way" classification of insulators and superconductors.

ACKNOWLEDGMENTS

The author has benefited with discussions with numerous friends and colleagues. We particularly thank our principal collaborators, Liang Fu, Eugene Mele, and Jeffrey Teo. This work has been supported by the National Science Foundation Grant DMR 0906175.

REFERENCES

[1] Thouless DJ, Kohmoto M, Nightingale MP, den Nijs M. Phys Rev Lett 1982;49:405.
[2] Wen XG. Adv Phys 1995;44:405.
[3] Kane CL, Mele EJ. Phys Rev Lett 2005;95:226801.
[4] Kane CL, Mele EJ. Phys Rev Lett 2005;95:146802.
[5] Bernevig BA, Hughes TA, Zhang SC. Science 2006;314:1757.
[6] König M, Wiedmann S, Brne C, Roth A, Buhmann H, Molenkamp LW, et al. Science 2007;318:766.
[7] Moore JE, Balents L. Phys Rev B 2007;75:121306(R).
[8] Roy R. Phys Rev B 2009;79:195322. Available from: arXiv:cond-mat/0607531.
[9] Fu L, Kane CL, Mele EJ. Phys Rev Lett 2007;98:106803.
[10] Fu L, Kane CL. Phys Rev B 2007;76:045302.
[11] Hsieh D, Qian D, Wray L, Xia Y, Hor YS, Cava RJ, et al. Nature 2008;452:970.
[12] Xia Y, Qian D, Hsieh D, Wray L, Pal A, Lin H, et al. Nat Phys 2009;5:398.
[13] Zhang H, Liu CX, Qi XL, Dai X, Fang Z, Zhang SC. Nature Phys 2009;5:438.
[14] Halperin BI. Phys Rev B 1982;25:2185.
[15] Tsui DC, Stormer HL, Gossard AC. Phys Rev Lett 1982;48:1559.
[16] Laughlin RB. Phys Rev Lett 1983;50:1395.
[17] Bloch FZ. Physik 1929;52:555.
[18] Nakahara M. Geometry, topology and physics. Bristol: Adam Hilger; 1990.
[19] Jackiw R, Rebbi C. Phys Rev D 1976;13:3398.
[20] Su WP, Schrieffer JR, Heeger AJ. Phys Rev Lett 1979;42:1698.
[21] Volkov BA, Pankratov OA. Pisma Zh Eksp Teor Fiz 1985;42:145; JETP Lett 1985;42:178.
[22] Fradkin E, Dagotto E, Boyanovsky D. Phys Rev Lett 1986;57:2967.
[23] Kaplan DB. Phys Lett B 1992;288:342.
[24] Volovik GE. The universe in a helium droplet. Oxford: Clarendon Press; 2003.
[25] Berry MV. Proc R Soc Lond A 1984;392:45.
[26] Blount EI. Solid State Phys 1962;13:305.
[27] Zak J. Phys Rev Lett 1989;62:2747.
[28] King-Smith RD, Vanderbilt D. Phys Rev B 1993;47:1651.
[29] Resta R. Rev Mod Phys 1994;66:899.
[30] Thouless DJ. Phys Rev B 1983;27:6083.

[31] Niu Q, Thouless DJ. J Phys A 1984;17:2453.
[32] Von Klitzing K, Dorda G, Pepper M. Phys Rev Lett 1980;45:494.
[33] Laughlin RB. Phys Rev B 1981;23:5632.
[34] Haldane FDM. Phys Rev Lett 1988;61:2015.
[35] Novoselov KS, Geim AK, Morozov SV, Jiang D, Katsnelson MI, Grigorieva IV, et al. Nature 2005;438:197.
[36] Zhang Y, Tan YW, Stormer HL, Kim P. Nature 2005;438:201.
[37] Geim AV, Novoselov KS. Nature Mater 2007;6:183.
[38] Castro Neto AH, Guinea F, Peres NMR, Novoselov KS, Geim AK. Rev Mod Phys 2009;81:109.
[39] DiVincenzo DP, Mele EJ. Phys Rev B 1984;29:1685.
[40] Semenoff GW. Phys Rev Lett 1984;53:2449.
[41] Wu C, Bernevig BA, Zhang SC. Phys Rev Lett 2006;96:106401.
[42] Fu L, Kane CL. Phys Rev B 2006;74:195312.
[43] Fukui T, Hatsugai Y. J Phys Soc Jpn 2007;76:053702.
[44] Fukui T, Fujiwara T, Hatsugai Y. J Phys Soc Jpn 2008;77:123705.
[45] Qi XL, Hughes TL, Zhang SC. Phys Rev B 2008;78:195424.
[46] Roy R. Phys Rev B 2009;79:195321. Available from: <arXiv:cond-mat/0604211>.
[47] Wang Z, Qi XL, Zhang SC. New J Phys 2010;12:065007.
[48] Teo JCY, Fu L, Kane CL. Phys Rev B 2008;78:045426.
[49] Zhang H, Liu CX, Qi XL, Dai X, Fang Z, Zhang SC. Nature Phys 2009;5:438.
[50] Pesin DA, Balents L. Nature Phys 2010;6:376.
[51] Guo HM, Franz M. Phys Rev Lett 2009;103:206805.
[52] Sheng DN, Weng ZY, Sheng L, Haldane FDM. Phys Rev Lett 2006;97:036808.
[53] Soluyanov AA, Vanderbilt D. Phys Rev B 2011;83:235401.
[54] Kohmoto M, Halperin BI, Wu YS. Phys Rev B 1992;45:13488.
[55] Ran Y, Zhang Y, Vishwanath A. Nat Phys 2009;5:298.
[56] Ringel Z, Kraus YE, Stern A. Phys Rev B 2012;86:045102.
[57] Mong RSK, Bardarson JH, Moore JE. Phys Rev Lett 2012;108:076804.
[58] Liu CX, Qi XL, Zhang SC. Physica E 2012;44:906.
[59] Lee PA, Ramakrishnan TV. Rev Mod Phys 1985;57:2871985.
[60] Suzuura H, Ando T. Phys Rev Lett 2002;89:266603.
[61] Nomura K, Koshino M, Ryu S. Phys Rev Lett 2007;99:146806.
[62] Fu L. Phys Rev Lett 2011;106:106802.
[63] Hsieh TH, Lin H, Liu J, Duan W, Bansil A, Fu L. Nature Commun 2012;3:982.
[64] Wan X, Turner AM, Vishwanath A, Savrasov SY. Phys Rev B 2011;83:205101.
[65] Yang KY, Lu YM, Ran Y. Phys Rev B 2011;84:075129.
[66] Burkov AA, Balents L. Phys Rev Lett 2011;107:127205.
[67] Young SM, Zaheer S, Teo JCY, Kane CL, Mele EJ. Phys Rev Lett 2012;108:140405.
[68] Schnyder AP, Ryu S, Furusaki A, Ludwig AWW. Phys Rev B 2008;78:195125.
[69] Schnyder AP, Ryu S, Furusaki A, Ludwig AWW. AIP Conf Proc 2009;1134:10.
[70] Kitaev A. AIP Conf Proc 2009;1134:22.
[71] Qi XL, Hughes TL, Raghu S, Zhang SC. Phys Rev Lett 2009;102:187001.
[72] Teo JCY, Kane CL. Phys Rev B 2010;82:115120.